Journal of Medicinal Chemistry

Article

Optimization of Fused-Bicyclic Allosteric SHP2 Inhibitors

Jeffrey Bagdanoff, Zhuoliang Chen, Michael G Acker, Ying-Nan P Chen, Homan Chan, Michaël Doré, Brant Firestone, Michelle Fodor, Jorge Fortanet, Murphy Hentemann, Mitsunori Kato, Robert Koenig, Laura R. LaBonte, Shumei Liu, Movarid Mohseni, Rukundo Ntaganda, Patrick Sarver, Troy Smith, Martin Sendzik, Travis Stams, Stan Spence, Christopher S. Towler, Hongyun Wang, Ping Wang, Sarah L. Williams, and Matthew J. LaMarche

J. Med. Chem., **Just Accepted Manuscript** • DOI: 10.1021/acs.jmedchem.8b01725 • Publication Date (Web): 28 Jan 2019

Just Accepted

ACS Publications

is published by the American Chemical Society. 1155 Sixteenth Street N.W., Washington, DC 20036

Optimization of Fused-Bicyclic Allosteric SHP2 Inhibitors

Jeffrey T. Bagdanoff,[a] Zhouliang Chen,[a] Michael Acker,[b] Ying-Nan Chen,[b] Homan Chan,[b] Michael Dore,[a] Brant Firestone,[b] Michelle Fodor,[c] Jorge Fortanet,[a] Murphy Hentemann,[b] Mitsunori Kato,[a] Robert Koenig,[a] Laura R. LaBonte,[d] Shumei Liu,[b] Movarid Mohseni,[e] Rukundo Ntaganda,[a] Patrick Sarver,[a] Troy Smith,[a] Martin Sendzik,[a] Travis Stams,[c] Stan Spence,[b] Christopher Towler,[e] Hongyun Wang,[b] Ping Wang,[b] Sarah L. Williams,[a] and Matthew J. LaMarche[,a]*

[a]Global Discovery Chemistry, [b]Oncology Disease Area, [c]Chemical Biology & Therapeutics, [d]Pharmacokinetic Sciences, Novartis Institutes for Biomedical Research, and [e]Chemical and Pharmaceutical Profiling, Novartis Pharmaceuticals, 250 Massachusetts Avenue, Cambridge, Massachusetts, 02139, United States

ABSTRACT

SHP2 is a non-receptor protein tyrosine phosphatase (PTP) within the MAPK pathway controlling cell growth, differentiation, and oncogenic transformation. SHP2 also participates in the programed cell death pathway (PD-1/PD-L1) governing immune surveillance. Small molecule inhibition of SHP2 has been widely investigated including our previous reports describing SHP099 (2), which binds to a tunnel-like allosteric binding site. To broaden our approach to allosteric inhibition of SHP2, we conducted additional hit finding, evaluation, and structure-based scaffold morphing. These studies, reported here in the first of 2 papers, led to the identification of multiple 5,6-fused bicyclic scaffolds which bind to the same allosteric tunnel as 2. These studies demonstrate the structural diversity permitted by the tunnel pharmacophore, and culminated in the identification of pyrazolopyrimidinones (e.g., SHP389, 1), that modulate MAPK signaling in vivo. These studies also served as the basis for further scaffold morphing and optimization, detailed in the following manuscript.

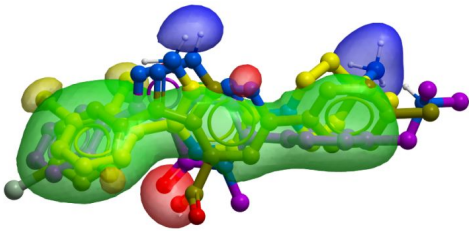

SHP2 Allosteric Pocket Pharmacophore Model

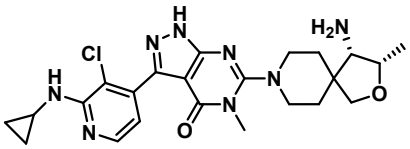

SHP389

INTRODUCTION

Activation of SHP2 phosphatase, encoded by the gene PTPN11, is genetically associated with multiple cancer types, including juvenile myelomonocytic leukemia, B-cell acute lymphoblastic leukemia, and acute myeloid leukemia.[1] SHP2 activating mutations also occur in solid tumors including lung adenocarcinoma, colon cancer, neuroblastoma, melanoma, and hepatocellular carcinoma.[2] SHP2 is a non-receptor protein tyrosine phosphatase composed of a C-terminal domain, a PTP domain, and two N-terminal Src homology 2 (SH2) domains. In its basal state, SHP2 adopts an autoinhibited conformation which associates the SH2 and PTP domains and restricts substrate access to the catalytic site. Activation of SHP2 occurs via binding of bis-phosphotyrosyl peptides (e.g., IRS-1) to the SH2 domains, disrupting the SH2-PTP association. The resulting

conformational change exposes the catalytic site and activates the enzyme by relieving auto-inhibition, promoting cancer dependent phosphatase activity.[3]

SHP2 is involved in numerous oncogenic cell signaling cascades, including the canonical RAS-ERK, PI3K-AKT, and JAK-STAT pathways.[4] The role of SHP2 in growth signaling via RAS/ERK/MAPK is more precisely defined, as SHP2 was reported to bind and dephosphorylate RAS and increase RAS–RAF association, activating downstream proliferative signaling.[5] Furthermore, the role of SHP2 in the T-cell programmed cell death/checkpoint pathway (PD–L1/PD–1) contributing to immune evasion is under investigation.[6,7] The PD-1/SHP2/STAT1/T-bet signaling axis mediates the suppressive effects of PD-1 on Th1 tumor immunity. Inhibition of PD-1 or SHP2 is therefore expected to restore Th1 immunity and T-cell activation, countering immunosuppression within the tumor microenvironment. Given recent clinical success of anti-PD-1 and PD-L1 therapeutics,[8] small molecule SHP2 inhibitors for cancer immunotherapy are highly desired clinical assets.[9]

Previously, we reported the identification of two new allosteric binding sites for SHP2 inhibition.[10,11] Initial medicinal chemistry efforts identified a moderately potent, selective, and

orally bioavailable inhibitor, SHP099 (**2**, Figure 1A).[12] **2** stabilizes an inactive conformation by concurrent binding to the interface of the N-terminal SH2, C-terminal SH2, and protein tyrosine phosphatase domains. The SHP099-inhibited conformation of SHP2 resembles the published inactive apo structure (PDB code 2SHP)[13] in which the *N*-terminal SH2 domain blocks the active site, resulting in autoinhibition of PTP activity. The continued optimization of the aminopyrazines will be described at a later time, separately from our published patent applications.[14] We have also described a second allosteric binding modality and found that dual small molecule allosteric binding via both mechanisms was possible.[11] Taken together, these pivotal publications and patent application disclosures have stimulated wide interest from the scientific community.[15] Both academic institutions[16] and biopharmaceutical companies[17] have disclosed drug discovery programs, exploiting related chemical matter which utilizes the initial allosteric modality. In this, the first of two articles, we report the design rationale and SAR studies which led to the identification of inhibitors across multiple fused-bicyclic chemical series, including the potent and selective pyrazolopyrimidinones, e.g., SHP389 (**1**). These studies also served as the basis for continued scaffold evolution and optimization.[18]

RESULTS AND DISCUSSION

As part of a comprehensive program directed at allosteric SHP2 inhibitors, we conducted a structure-based prioritization of chemical matter identified through high-throughput screening.[10] Comparison of the binding pose of our previously disclosed

SHP2 inhibitor **2** with the SHP2-cocrystal structure of HTS hits **3** and **4** (PDB codes *5EHR*, *6MD9*, *6MDA*, respectively) revealed several conserved protein-ligand interactions (Figure 1). For example, all three ligands engage a *Pi*-cation interaction between the haloarene and the guanidinium of R111. The haloarene of each ligand is also framed by Van der Waals interactions with the lipophilic sidechains P491 and L254. In the case of pyrazolopyridine **4**, the pendant carboxylate accesses an additional water-mediated interaction with R111 and a direct polar interaction with N217. Both **2** and **4** individually form an additional polar interaction with the back-bone carbonyl of E250 with aniline and pyrazole proton donors, respectively, while **3** lacks the required H-bond donor. Of the three structures, only **2** contained a hydrogen bond donor contacting the F113 backbone carbonyl.

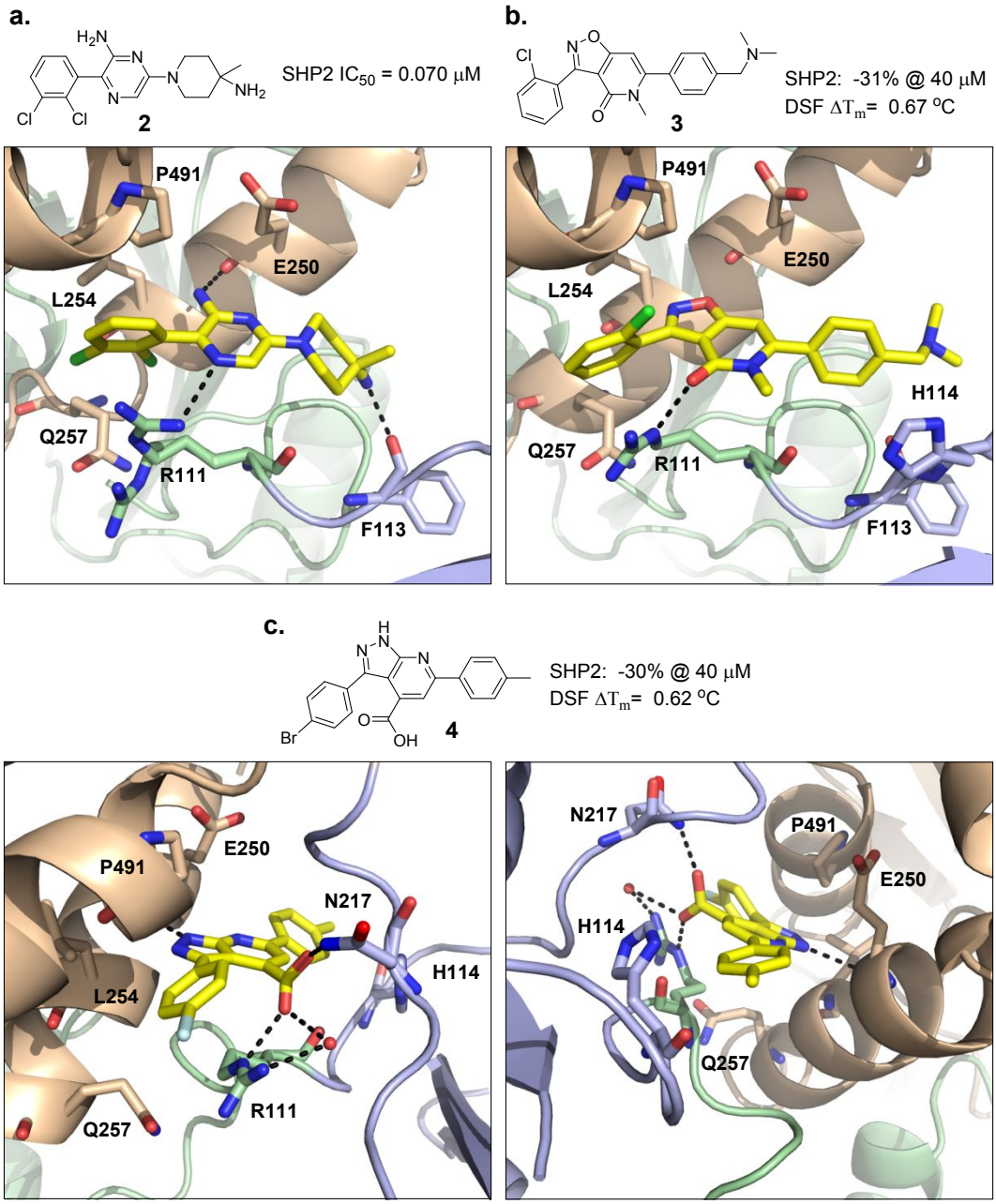

Figure 1. SHP2 binding interactions with (a) **2**, (b) **3** and (c) **4**. PDB codes: *5EHR*, *6MD9*, *6MDA*, respectively.

A pharmacophore model adopted from **2**, **3** and **4** (Figure 2A) broadly characterized SHP2 allosteric pocket ligands as being composed of: an H-bond donor to

the backbone carbonyl of E250; an H-bond acceptor to the guanidinium[19] of R111; an H-bond donor to F113; a *Pi*-cation interaction with R111; Van der Waals interactions between the pendant arene and lipophilic residues P491 and L254. Accounting for all the interactions implied by this model, pyrazolopyrimidinone **5** was envisioned which combines the chloroarene and amine features of **2**, the 5,6-fused, bicyclic core of **3** and **4**, and the E250 binding N-H donor present in **2** and **4**. Consistent with our design hypothesis, pyrazolopyrimidinone **5** was found to potently inhibit the biochemical activity of SHP2 (Figure 2B, IC_{50} = 0.067 μM), and inhibited SHP2 mediated phosphorylation of ERK kinase (IC_{50} = 0.746 μM) and demonstrated a modest antiproliferative effect in a KYSE520 cell line (IC_{50} = 4.76 μM). Analysis of the co-crystal structure of **5** in the SHP2 allosteric binding pocket (PDB code *6MDB*, Fig 2C) confirmed engagement of all interactions implicated in the pharmacophore model (*vide supra*). In addition to these predicted interactions, the pyrimidinone carbonyl participated in a water-mediated interaction with N127 and T219 while the tertiary amine donated a proton in an H-bond to E249. Compound **5** also had an acceptable pharmacokinetic profile in mouse (Cl 34 mL/min/kg, 25% oral bioavailability), supporting the further optimization of the

pyrazolopyrimidinone class for improved potency and selectivity over the hERG channel (IC_{50} = 0.200 μM).

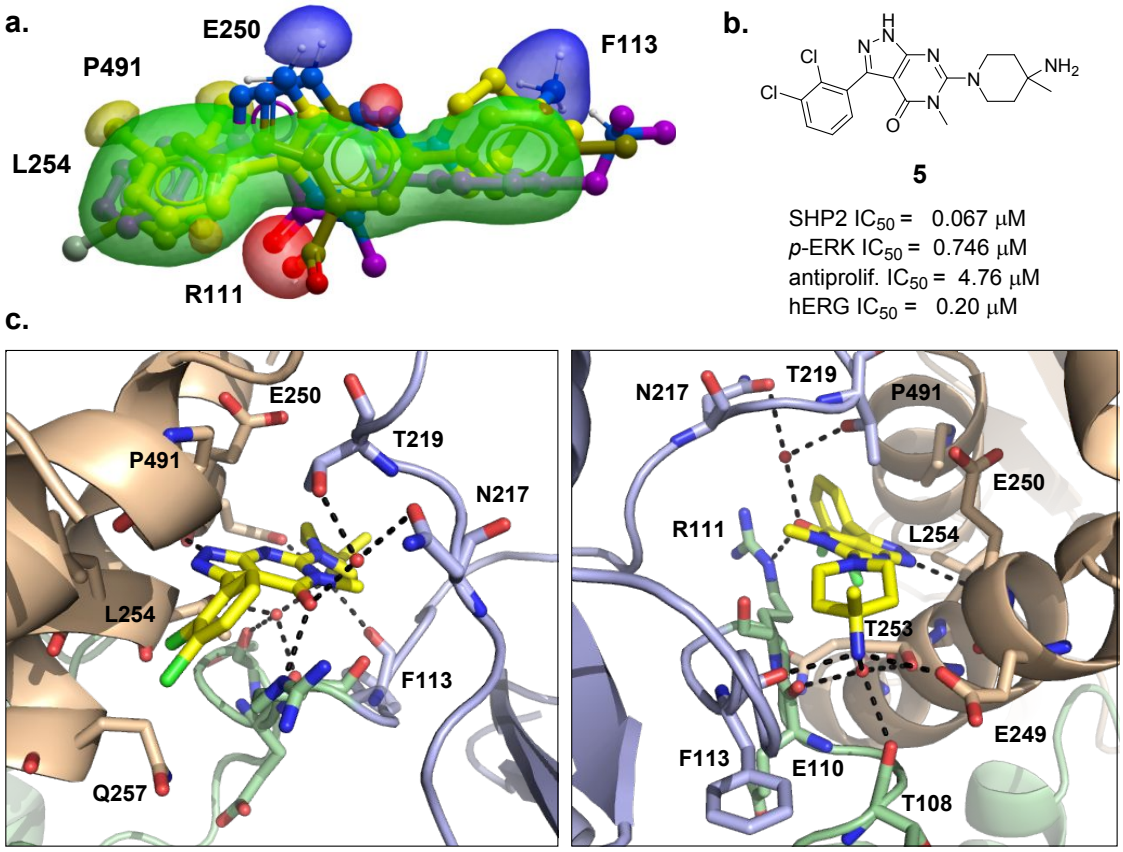

Figure 2. (a) Pharmacophore model derived from **2**, **3** and **4**. Blue is H-bond donor. Red is H-bond acceptor. Green is lipophilic. (b) In vitro profile of designed ligand **5**. (c) Cocrystal of **5** in SHP2 allosteric pocket (PDB code *6MDB*).

The synthesis of pyrazolopyrimidinones began with the reaction of 6-chlorouracil **6** with hydrazine hydrate to provide intermediate **7** after condensation with 4-methoxybenzaldehyde. Alternatively, the benzyl protected intermediate **8** was accessed by a similar sequence using benzaldehyde. Piperidine catalyzed cyclocondensation of **7**

with an aromatic aldehyde completed the carbon framework present in intermediate **9**. Intermediate **8** was derivatized by parallel synthetic strategies, one of which required generation of the halide **10**. Intermediates **8**, **9** and **10** were further advanced by installation of aliphatic amines under peptide coupling or SnAr conditions to provide after deprotection, final pyrazolopyrmidinone products **11-25**.

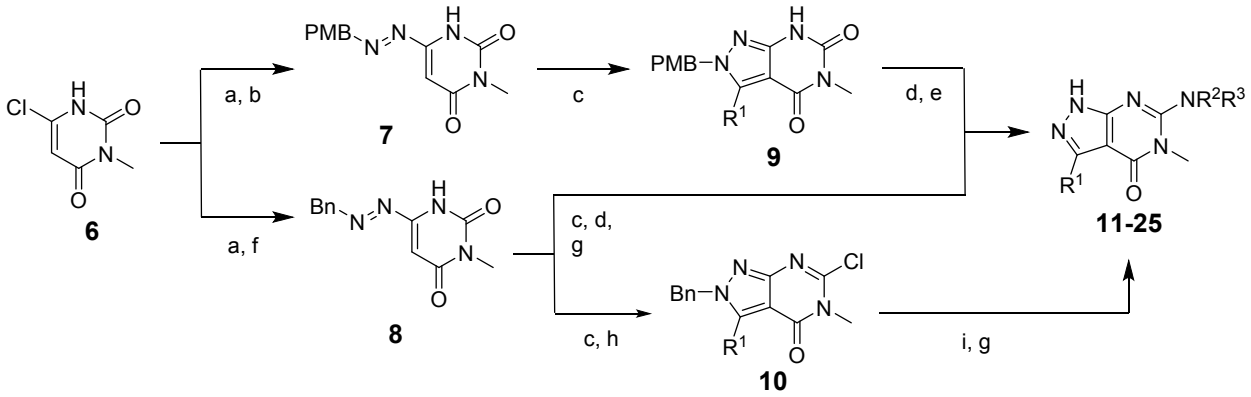

Scheme 1. General synthesis of pyrazolopyrimidinones.[a]

[a]Reagents and conditions: (a) H_2NNH_2-H_2O, EtOH, 80 °C; (b) 4-methoxybenzaldehyde, MeOH; (c) R^1COH, piperidine, DMF, *i*-PrOH, 90 °C; (d) $R^2R^3NH_2$, BOP, DMF (e) TFA, DCE, 70 °C; (f) benzaldehyde, MeOH; (g) *t*-BuONa, DMSO, O_2; (h) $POCl_3$, $Me4N^+I^-$, 100 °C; (i) $R^2R^3NH_2$, DIPEA, NMP, μ-wave, 120 °C.

We observed water with variable weak density across co-crystal structures in the vicinity of the basic amine of **5** (e.g., Figure 2C). Elaboration of the amine substituent[20] provided a handle for modulating the biochemical and cellular potency of prototype **5**

(Table 1). Extending the basic amine in order to displace the proposed water, returned a modest improvement in SHP2 biochemical inhibition with improvement of hERG selectivity (e.g., compound **11**). However, the modest biochemical improvement did not clearly benefit either the *p*-ERK or KYSE proliferation cellular assays. Cyclization to the spiro[4.5]-amine (**12**) provided little additional benefit to SHP2 biochemical potency but provided a >10-fold improvement in the *p*-ERK and KYSE antiproliferation cellular assays. This was likely due to an increase in affinity, as the biochemical IC_{50} ranged from 0.009 to 0.045 μM (the average of three experiments shown in table 1, 0.031 μM). Tetrahydrofuran analog **13** was designed to mitigate amine basicity, but was less potent than **12** by all measures. **13** presented an improved lipophilic efficiency (LipE), owing to a one log reduction in lipophilicity. The expected reduction in lipophilicity and basicity provided by ether **13** produced only a minor benefit to hERG inhibition. In an attempt to restore cellular potency by rebalancing lipophilicity, the spirocyclic ether was methylated to provide **14**. This maneuver improved both the *p*-ERK modulation (IC_{50} = 0.012 μM) and enhanced by 10-fold the antiproliferative activity against KYSE520 cells (IC_{50} = 0.167 μM).

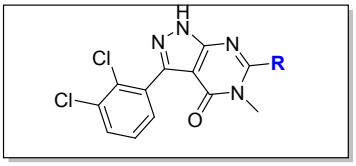

Compound	R	SHP2 IC_{50} (μM)	*p*-ERK IC_{50} (μM)	antiproliferation IC_{50} (μM)	cLogP/LipE	hERG IC_{50} (μM)
11		0.034	0.355	13.49	3.1/3.1	0.98
12	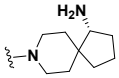	0.031	0.030	0.465	3.4/3.2	0.25
13	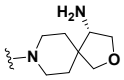	0.050	0.123	1.73	2.3/4.7	0.93
14	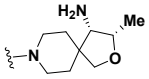	0.028	0.012	0.167	2.9/4.0	0.29

Table 1. Optimization of the spirocyclic amine for potency and hERG selectivity.

In light of the promising biochemical and cellular data, we sought to mitigate the hERG liability initially observed in the dofetilide binding assay and later confirmed by Q-Patch (**14**: IC_{50} = 0.70 μM). Bearing in mind our SHP2 allosteric pocket pharmacophore model (Figure 2A), we modeled potential binding interactions for various alternative heterocyclic cores within the SHP2 allosteric pocket. Our structural analysis indicated that retraction of the H-bond acceptor carbonyl presented by the pyrazolopyrimidinone core, as exemplified by pyrazolopyrazine **15** (Table 2), would retain the native donor-acceptor SHP2 interactions. A docking analysis of **15** in the SHP2 allosteric pocked

further supported this hypothesis; the pyrazine nitrogen modeled within Van der Waals radius for interaction with R111 (Figure 3). Consistent with the elevated lipophilicity, **15** was a remarkably potent SHP2 inhibitor (biochemical IC_{50} = 0.006 μM) with substantial cellular potency (*p*-ERK IC_{50} = 0.031 μM, KYSE520 antiproliferative IC_{50} = 0.46 μM), but also potently inhibited the hERG channel (IC_{50} = 0.004 μM). While the pyrazole N-H of the pyrazolopyrimidine heterocycle was deemed important due to the E250 backbone carbonyl contact, other heteroatoms in the core formed no H-bond acceptor interactions and were removed. The resulting pyrrolopyrazine, **16,** was moderately potent in biochemical (IC_{50} = 0.039 μM) and *p*-ERK KYSE520 cellular (IC_{50} = 0.473 μM) assays. Unfortunately, neither **15** nor **16** improved the selectivity over the hERG channel.

Compound	Structure	SHP2 IC_{50} (μM)	*p*-ERK IC_{50} (μM)	antiproliferation IC_{50} (μM)	cLogP/LipE	hERG IC_{50} (μM)
15	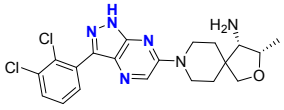	0.006	0.031	0.46	3.9/4.3	0.004
16	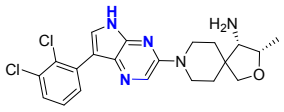	0.039	0.484	--	4.1/3.3	0.007

Table 2 Core 5,6-fused bicycle SAR.

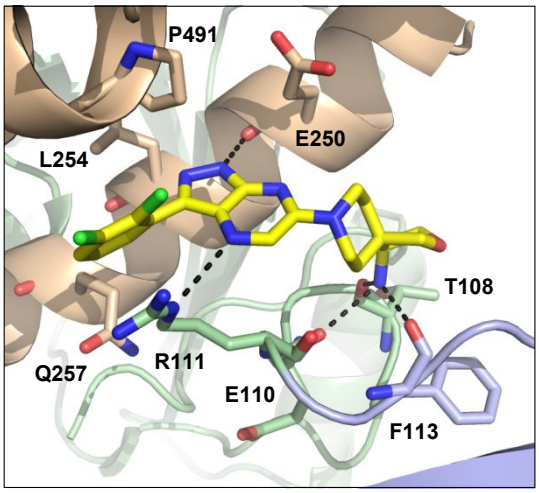

Figure 3. **15** modeled into the SHP2 allosteric binding pocket preserves R111 interaction. (Docking model built from PDB code *6MDB*)

After optimizing the spirocyclic amine for biochemical and cellular potency and deprioritizing core heterocycle modifications as a means for improving hERG inhibition, we next focused our SAR study at the pendant chloroarene. Substituting the dichlorophenyl subunit in **11-16** with dichloropyridine **17** (Table 3) moderately mitigated hERG inhibition (IC_{50} = 1.2 μM). The heteroatom insertion substantially reduced lipophilicity by ~1.5 log units (vs. matched pair **14**, Table 1) resulting in improved lipophilic efficiency (**17**: LipE = 4.9). Compound **17** had moderate *p*-ERK cellular potency (*p*-ERK IC_{50} = 0.093 μM), and the antiproliferative effects were blunted (antiproliferative IC_{50} = 2.6

μM). The net benefits of tuning polarity and lipophilicity via the pendant arene prompted further investigation.

The unsubstituted pyridine **18** delivered superior biochemical potency (IC_{50} = 0.008 μM) with no discernable hERG signal and high lipE (5.9). However, **18** did not deliver a concomitant improvement in cellular potency, presumably due to the lower membrane permeability resulting from a log unit reduction in lipophilicity relative to dichloropyridine **17**. Replacement of the 2,3-dichloropyridine motif with 2-amino, 3-chloro aminopyridine **19** significantly reduced hERG activity and provided a new vector for synthetic elaboration. Appending small lipophilic groups including methyl (**20**) and cyclopropyl (**1**) improved SHP2 biochemical and cellular potency in trend with increasing lipophilicity. Cyclobutane analog **21** resulted in a steep reduction in biochemical and cellular potency, presumably due to increased steric bulk. Overall, we observed that hERG IC_{50} roughly tracked with lipophilicity, where progressively lipophilic molecules displayed an increasingly severe hERG liability.

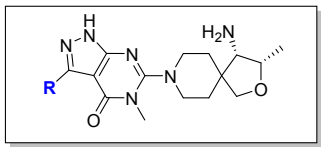

Compound	R	SHP2 IC_{50} (μM)	*p*-ERK IC_{50} (μM)	antiproliferation IC_{50} (μM)	cLogP/LipE	hERG IC_{50} (μM)
17		0.028	0.093	2.60	1.5/4.9	1.2
18		0.008	0.129	1.26	0.3/5.9	>30
19	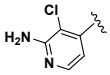	0.032	0.103	1.20	0.6/6.4	>30
20	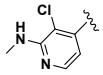	0.055	0.022	0.37	1.4/5.7	>30
1	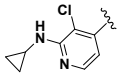	0.036	0.036	0.36	2.0/4.7	17.0
21	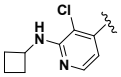	0.350	0.260	0.38	2.3/4.4	1.9
22	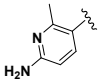	0.037	0.038	0.66	0.2/5.8	6.6
23	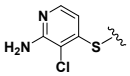	0.027	0.096	0.72	1.2/5.7	>30

Table 3. Optimization of the pyridine substituent for potency and hERG selectivity.

While the collection of heteroatoms presented by 2-amino, 3-chloropyridine might conceivably access specific interactions within the SHP2 allosteric pocket, our SAR suggested otherwise. For example, reconfiguration of the heteroatom presentation, as in regioisomeric aminoyridine **22**, also delivered promising biochemical potency that was robustly reproduced in cells. That **22** was sufficiently permeable for cellular potency was

unexpected given the low clogP. For comparison, **22** was substantially less lipophilic than **1** (cLogP = 1.2 vs 2.0, respectively), yet delivered equivalent cellular potency. However, the lower lipophilicity of **22** did not fully relieve hERG promiscuity (IC_{50} = 6.6 μM).

More dramatic variations of the pyrazolopyrimidinone substructure were also anticipated to bind the SHP2 allosteric tunnel. For example, a docking study (Figure 4) supported the hypothesis that substitution of the Ar-Ar bond present in **19** with the Ar-S-Ar motif, as is present in the HTS screening hit **24**, could satisfy the pharmacophore model developed for the 5,6-fused bicyclic chemical series (Figure 2A). The structural overlay demonstrated rough alignment of the core heterocycle and flanking arene substructure. Bearing in mind these design considerations, **23** was characterized as a potent biochemical inhibitor (IC_{50} = 0.027 μM). Cellular characterization further demonstrated the potency of **23** in the *p*-ERK assay (IC_{50} = 0.096 μM) and the KYSE antiproliferation assay (IC_{50} = 0.72 μM). As previously observed, the 2-amino, 3-chlopropyridine motif correlated with low hERG affinity (IC_{50} > 30 μM).

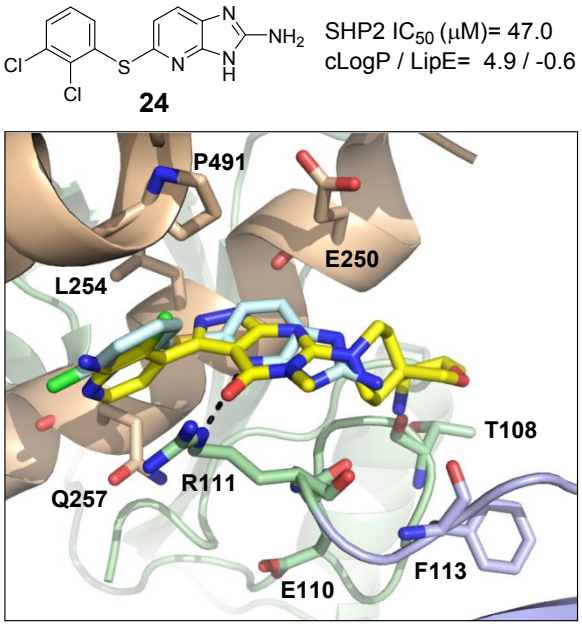

Figure 4. Overlay of **24** and **19** supports binding hypothesis of hybrid **23**. PDB code of SHP2-**24** *6MDD*.

Considering the substantial structural changes made to the flanking substituents of the root design **5** (Figure 2), we were motivated to better understand the nature of the evolving protein-ligand interactions. To this end, a cocrystal structure of **1** was obtained (Figure 5). The major polar interactions included those anticipated by the pharmacophore model (Figure 2A): a polar interaction between the pyrazolopyrimidinone carbonyl and R111; a polar interaction between pyrazolopyrimidinone N-H and E250; a *Pi*-cation interaction between the 2-amino, 3-chloropyridine heterocycle and R111; an H-bond

donor interaction between the spirocyclic amine and F113. Previously unobserved interactions included water mediated interactions between the pyrazolopyrimidinone carbonyl, T219, and N217, as well as polar interactions between the spirocyclic amine and the F113, E110, and T108 triad. Conspicuously absent were polar interactions with the 2-aminocyclopyropyl, 3-chloropyridine substructure present in **1**. This observation helped rationalize the equivalent potency of structurally diverse regioisomeric aminopyridine **22**. Lacking donor-acceptor interactions in this region of the SHP2 allosteric binding pocket, regioisomeric aminopyridines produced comparable biochemical inhibition. A key observation from Table 2 is that the aminopyridine based analogs delivered hERG selective SHP2 inhibitors.

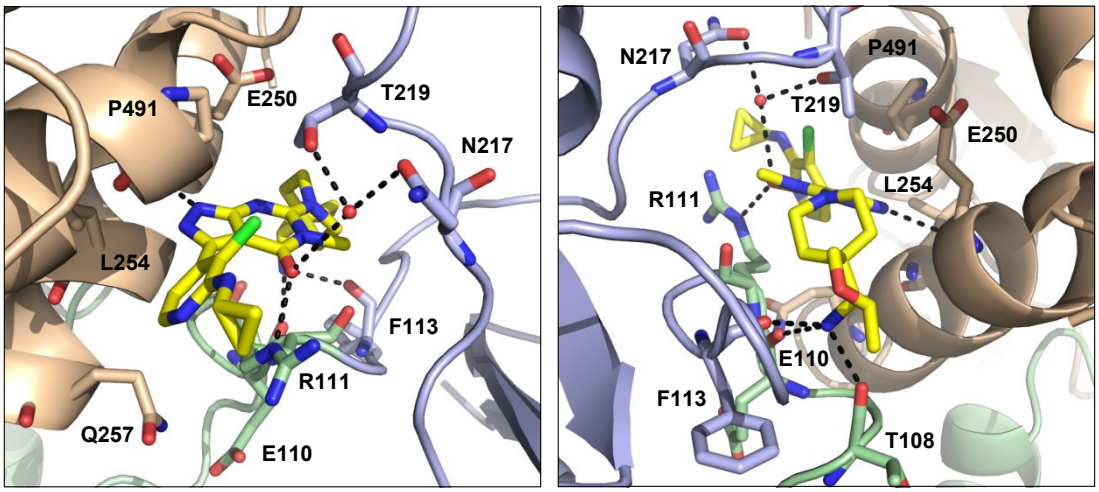

Figure 5. Co-crystal structure of **1** in the SHP2 allosteric pocket (PDB code *6MDC*).

On the basis of their overall in vitro profile, **1** and **14** were prioritized for additional profiling, and were selective versus a panel of 30 GPCRs, ion channels, nuclear receptors, transporters, enzymes and kinases (IC_{50} >30 μM). While preliminary evaluation of hERG binding by a dofetilide binding assay indicated **1** weakly inhibited hERG (IC_{50} = 17 μM) a more detailed evaluation by Q-Patch demonstrated that the compound did not engage a functional hERG interaction (IC_{50} >30 μM). The *in vitro* metabolic clearance profile (mouse ER = 27%, rat ER = 46%) and clean CYP450 profile (CYP 3A4, 2D6 and 2C9 IC_{50} >50 μM) of **1** encouraged further *in vivo* evaluation. Compound **1** was dosed IV/PO at 1/5 mg/kg, respectively, to male Sprague Dawley rats in a crossover study design. Compound **1** demonstrated a moderate-high clearance (~83% hepatic extraction) which was under predicted in vitro by rat liver microsomes (Cl = 26.1 μL/min/mg, $T_{1/2}$ = 53.2 min) assuming a hepatic blood flow of 55 mL/min/kg. The volume of distribution was moderate-high (3.9 L/kg) with a terminal half-life of 2.7 h. Following oral administration, the compound had low oral bioavailability (~2 %F) which is

consistent with poor in vitro permeability (PAMPA). This limited exposure therefore prevented further pharmacologic evaluation of **1** in a mouse tumor xenograft model.

We thus turned to **14**, a potent compound (KYSE520 *p-ERK* IC_{50} = 0.093 μM; antiproliferative IC_{50} = 0.170 μM) with a less selective profile (hERG IC_{50} = 0.29 μM) in order to characterize *in vivo* pharmacodynamic markers. In addition to its robust antiproliferative effects, **14** had acceptable stability in mouse liver microsomes (Cl = 36.8, μL/min/mg, $T_{1/2}$ = 60.2 min) and was sufficiently soluble (pH = 6.8 equilibrium solubility = 0.42 mM) to enable PK pharmacokinetic evaluation. Compound **14** was dosed IV/PO at 1 and 5 mg/kg, respectively, to male Sprague Dawley rats in a crossover study design. Compound **14** demonstrated high clearance (> hepatic blood flow), a high volume of distribution (10.5 L/kg), a moderate half-life ($T_{1/2}$ = 4.6 h), and moderate oral bioavailability (F = 51 %). Additionally, the PK and *in vivo* activity of **14** was assessed in mice subcutaneously implanted with the KYSE520 carcinoma cell line. Tumor-bearing mice were given a single oral dose of **14** at 10, 30 and 100 mg/kg. Free concentrations of **14** (89% mouse plasma protein bound) correlated well with the MAPK pharmacodynamic markers, *p*-ERK and DUSP6 (Figure 3). The maximal PD effect, as determined by *p*-ERK and DUSP6

concentrations in blood, was observed at 100 mg/kg for at least 8 hours, with PD rebound correlating with clearance of **14**.

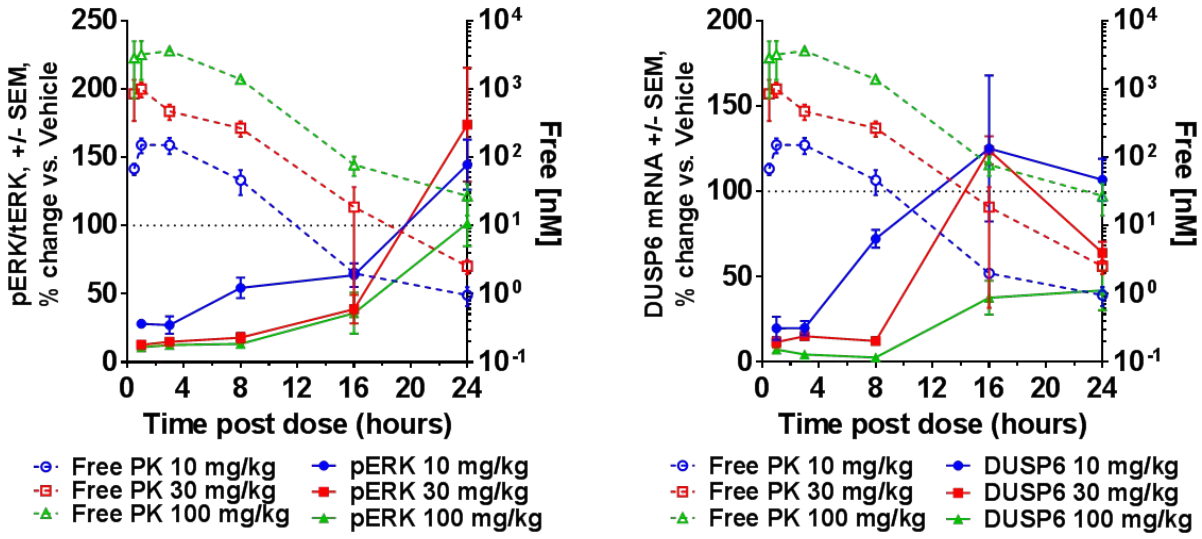

Figure 3. PK/PD of **14** at 10, 30, and 100 mg/kg in mice bearing KYSE520 xenografts.

CONCLUSION

As part of a program directed at identifying allosteric SHP2 inhibitors, we successfully merged the salient structural features of established SHP2 ligands (e.g., **2**) with new HTS hits (e.g., **3**, **4**, **25**). This pharmacophore blending exercise produced pyrazolopyrimidinone **5**, which contains a 5,6-fused heterocycle that was confirmed by X-ray crystallography to bind to the same allosteric tunnel site as **2**. Extension and conformational restriction of the amine substituent led to the identification of **14**, which

elicited a robust PK-PD correlation in a mouse tumor xenograft model. This result further motivated us to improve the poor hERG selectivity associated with the 5,6-fused bicyclic series. Substitution of the pyrazolopyrimidinone core with other 5,6-fused heterocycles provided new potent allosteric scaffolds with similar binding modalities, but failed to address the hERG selectivity. A more successful approach was found through modification of the pendant chloroarene presented by **14**. Decoration of the chloroarene with nitrogen heteroatoms, as in aminopyridine **19**, provided a firm handle for improving hERG selectivity and a new vector for synthetic manipulation. Continued experimentation demonstrated that cyclopropane **1** successfully balanced high biochemical and cellular potency with impressive hERG selectivity (Q-Patch IC_{50} >30 μM). While our *in vitro* objectives were met in this study, compound **1** ultimately fell short of demonstrating sufficiently robust oral bioavailability to support PK/PD and tumor efficacy studies. Taken together, these investigations demonstrated the structural determinants governing efficient, cellularly potent, allosteric SHP2 binders from various 5,6-fused bicyclic frameworks, a clear strategy for effectively improving hERG selectivity, and ultimately served as basis for further optimization.[18]

EXPERIMENTAL SECTION

Compound synthesis and characterization. Compound purity was assessed by HPLC to confirm >95% purity. All solvents employed were commercially available anhydrous grade, and reagents were used as received unless otherwise noted. A Biotage Initiator™ Sixty system was used for microwave heating. Flash column chromatography was performed on either an Analogix Intelliflash 280 using Si 50 columns (32-63 μm, 230-400 mesh, 60Å) or on a Biotage SP1 system (32-63 μm particle size, KP-Sil, 60 Å pore size). Preparative high pressure liquid chromatography (HPLC) was performed using a Waters 2525 pump with 2487 dual wavelength detector and 2767 sample manager. Columns were Waters C18 OBD 5μm, either 50x100 mm Xbridge or 30x100 mm Sunfire. NMR spectra were recorded on a Bruker AV400 (Avance 400 MHz) or AV600 (Avance 600 MHz) instruments. Analytical LC-MS was conducted using an Agilent 1100 series with UV detection at 214 nm and 254 nm, and an electrospray mode (ESI) coupled with a Waters ZQ single quad mass detector. One of three methods was used: Method A) 5-95 % acetonitrile/H_2O with 5 mM ammonium formate with a 2 min run, 3 μL injection through an inertisil C8 3 cm x 5 mm x 3μm; Method B) 20-95 % acetonitrile/H_2O with 10 mM ammonium hydroxide with a 2 min run, 3 μL injection through an inertisil C8 3 cm x 5 mm x μm; Method C) 5-95 % acetonitrile/H_2O with 0.05 % trifluoroacetic acid with a 2 min run, 3 μL injection through an Sunfire C18 3.5 μm 3.0 x 30 mm. Purity of all tested compounds was determined by LC/ESI-MS Data recorded using an Agilent 6220 mass spectrometer with electrospray ionization source and Agilent 1200 liquid chromatography. The mass accuracy of the system has been found to be < 5 ppm. HPLC separation was performed at 75 mL/min flow rate with the indicated gradient

within 3.5 min with an initial hold of 10 seconds. 10 mM ammonia hydroxide or 0.1 M TFA was used as the modifier additive in the aqueous phase.

Synthesis of SHP389: 6-((3S,4S)-4-amino-3-methyl-2-oxa-8-azaspiro[4.5]decan-8-yl)-3-(3-chloro-2-(cyclopropylamino)pyridin-4-yl)-5-methyl-2,5-dihydro-4H-pyrazolo[3,4-d]pyrimidin-4-one (1). Hydrazine hydrate (9.17 mL, 187 mmol) was added to a solution of 6-chloro-3-methyluracil (10 g, 62.3 mmol) in ethanol (200 mL). The resulting mixture was stirred at 80 °C. The slurry became increasingly thick over the course of 10 min. The heating was continued for 1 h, then the heat bath was removed and the reaction mixture was allowed to cool to room temperature for 1 h. The resulting suspension was filtered and the filter cake was dried under vacuum. The intermediate 6-hydrazinyl-3-methylpyrimidine-2,4(1*H*,3*H*)-dione was obtained as a white powder (9.7 g, 100% yield) and was used directly in the next transformation.

To a suspension of 6-hydrazinyl-3-methylpyrimidine-2,4(1*H*,3*H*)-dione (5.26 g, 33.7 mmol) in MeOH (25 mL) was added 2,3-dichlorobenzaldehyde (5.50 g, 40.4 mmol). The result mixture was stirred at room temperature for 30 min. The slurry became very thick, and was diluted with methanol (25 mL) to facilitate stirring. The reaction was maintained for an additional 30 min, at which point the reaction was complete by LCMS.

The slurry was filtered and the filter cake was dried under vacuum for 16 h to provide 6-((4-methoxybenzyl)diazenyl)-3-methylpyrimidine-2,4(1*H*,3*H*)-dione as a white solid (8.0 g, 87% yield). LCMS: *m/z* 280 $(M+1)^+$, R_t=0.43 min.

To a suspension of 6-((4-methoxybenzyl)diazenyl)-3-methylpyrimidine-2,4(1*H*,3H)-dione (0.68 g, 2.479 mmol) in DMF (8 mL) and *i*-PrOH (4 mL) was added 2,3-dichloroisonicotinaldehyde (0.436 g, 2.479 mmol) and piperidine (0.241 mL, 2.430 mmol). The result mixture was stirred at 85 °C for 1 h. At completion, the reaction mixture was partitioned between water (50 mL) and ethyl acetate (50 mL). The layers were separated and the aqueous layer was washed with ethyl acetate (50 mL). The combined organics were washed with brine (40 mL), dried with Na_2SO_4, filtered and concentrated. The crude was purified by flash chromatography over silica gel (0-10% methanol/DCM eluent) to afford 3-(2,3-dichloropyridin-4-yl)-2-(4-methoxybenzyl)-5-methyl-2*H*-pyrazolo[3,4-*d*]pyrimidine-4,6(5*H*,7*H*)-dione as a yellow solid (420 mg, 39% yield, 90% purity). LCMS: *m/z* 432 $(M+1)^+$, R_t= 1.29 min.

To a suspension of 3-(2,3-dichloropyridin-4-yl)-2-(4-methoxybenzyl)-5-methyl-2*H*-pyrazolo[3,4-*d*]pyrimidine-4,6(5*H*,7*H*)-dione (500 mg, 1.16 mmol) in DMSO (3 mL) was added cyclopropanamine (330 mg, 5.78 mmol). The resulting mixture was microwave heated to 140 ^{o}C for 20 min. At completion, the reaction was partitioned between water (15 mL) and ethyl aceate (15 mL). The organics were separated and the aqueous layer was washed with ethyl acetate (2 x 10 mL). The combined organics were washed with brine, dried over Na_2SO_4 and concentrated. The crude was purified by flash chromatography over silica gel (0-70% ethyl acetate/heptane eluent) to provide 3-(3-chloro-2-(cyclopropylamino)pyridin-4-yl)-2-(4-methoxybenzyl)-5-methyl-2,7-dihydro-4*H*-pyrazolo[3,4-*d*]pyrimidine-4,6(5*H*)-dione (280 mgs, 53% yield). LCMS: *m/z* 453.2 $(M+1)^+$, R_t=0.65 min.

To a solution of 3-(3-chloro-2-(cyclopropylamino)pyridin-4-yl)-2-(4-methoxybenzyl)-5-methyl-2,7-dihydro-4*H*-pyrazolo[3,4-*d*]pyrimidine-4,6(5*H*)-dione (280 mgs, 0.618 mmol) in DMF (2 mL) was added (benzotriazol-1-yloxy)tris(dimethylamino)phosphonium hexafluorophosphate (820 mgs, 1.855 mmol).

After 15 min, the mixture was treated with (3*S*,4*S*)-3-methyl-2-oxa-8-azaspiro[4.5]decan-4-amine (195 mgs, 0.804 mmol) and 1,8-diazabicyclo[5.4.0]undec-7-ene (753 mgs, 4.95 mmol). At completion, the reaction was partitioned between water (15 mL) and ethyl acetate (15 mL). The organics were separated and the aqueous phase was washed with ethyl acteate (2 x 10 mL). The combined organics were washed with brine (10 mL), dried over $MgSO_4$ and concentrated. The crude was purified by flash chromatography over silica gel (0-5% MeOH/DCM eluent) to provide 6-((3*S*,4*S*)-4-amino-3-methyl-2-oxa-8-azaspiro[4.5]decan-8-yl)-3-(3-chloro-2-(cyclopropylamino)pyridin-4-yl)-2-(4-methoxybenzyl)-5-methyl-2,5-dihydro-4*H*-pyrazolo[3,4-*d*]pyrimidin-4-one (170 mg, 45% yield). LCMS: *m/z* 606.0 $(M+1)^+$, R_t=0.72 min.

A solution of 6-((3*S*,4*S*)-4-amino-3-methyl-2-oxa-8-azaspiro[4.5]decan-8-yl)-3-(3-chloro-2-(cyclopropylamino)pyridin-4-yl)-2-(4-methoxybenzyl)-5-methyl-2,5-dihydro-4*H*-pyrazolo[3,4-*d*]pyrimidin-4-one (170 mg, 0.281 mmol) in TFA (3 mL) and DCE (3 mL) was heated to 70 °C. After 2 h, the reaction was concentrated, then dissolved in DCM, treated with heptane and concentrated. The crude was purified by prep HPLC to provide 6-

((3*S*,4*S*)-4-amino-3-methyl-2-oxa-8-azaspiro[4.5]decan-8-yl)-3-(3-chloro-2-(cyclopropylamino)pyridin-4-yl)-5-methyl-2,5-dihydro-4*H*-pyrazolo[3,4-*d*]pyrimidin-4-one (53 mg, 38% yield). ^{1}H NMR (400 MHz, METHANOL-d_4) δ ppm 8.04 (d, *J* = 5.05 Hz, 1 H), 6.76 (d, *J* = 5.31 Hz, 1 H), 4.20 - 4.26 (m, 1 H), 3.85 (d, *J* = 8.59 Hz, 1 H), 3.70 (d, *J* = 8.84 Hz, 1 H), 3.43 - 3.53 (m, 7 H), 2.99 - 3.17 (m, 5 H), 2.74 (tt, *J* = 7.01, 3.47 Hz, 1 H), 1.86 - 2.06 (m, 3 H), 1.67 - 1.82 (m, 3 H), 1.22 (d, *J* = 6.57 Hz, 4 H), 0.79 - 0.87 (m, 2 H), 0.55 - 0.63 (m, 2 H). LCMS: *m/z* 485.3 $(M+1)^+$, R_t=0.88 min.

Protein Expression and Purification. The gene encoding human SHP2 from residues Met1−Leu525 was inserted into a pET30 vector. A coding sequence for a 6× histidine tag followed by a TEV protease consensus sequence was added 5′ to the SHP2 gene sequence. The construct was transformed into BL21 Star (DE3) cells and grown at 37°C in Terrific Broth containing 100 μg/mL kanamycin. At an OD600 of 4.0, SHP2 expression was induced using 1 mM IPTG. Cells were harvested following overnight growth at 18 °C. Cell pellets were resuspended in lysis buffer containing 50 mM Tris-HCl, pH 8.5, 25 mM imidazole, 500 mM NaCl, 2.5 mM MgCl2, 1 mM TCEP, 1 μg/mL DNase1, and complete EDTA-free protease inhibitor and lysed using a microfluidizer, followed by ultracentrifugation. The supernatant was loaded onto a HisTrap HP chelating column in 50 mM Tris-HCl, 25 mM imidazole, 500 mM NaCl, 1 mM TCEP and protein was eluted with the addition of 250 mM imidazole. The N-terminal histidine tag was removed with an overnight incubation using TEV protease at 4 °C. The protein was subsequently diluted to 50 mM NaCl with 20 mM Tris-HCl, pH 8.5, 1 mM TCEP, then applied to a HiTrap Q FastFlow

column equilibrated with 20 mM Tris, pH 8.5, 50 mM NaCl, 1 mM TCEP. The protein was eluted with a 10 column volume gradient from 50 to 500 mM NaCl. Fractions containing SHP2 were pooled and concentrated then loaded onto a HiLoad Superdex200 PG 16/100 column, exchanging the protein into the crystallization buffer, 20 mM Tris-HCl, pH 8.5, 150 mM NaCl, and 3 mM TCEP. The protein was concentrated to 15 mg/mL for use in crystallization. Crystallization, DSF, and high throughput screening assays used the 1−525 construct of SHP2, while biochemical assays used the 2−593 construct.

Biochemical Assay. SHP2 is allosterically activated through binding of bis-tyrosyl-phorphorylated peptides to its Src Homology 2 (SH2) domains. The latter activation step leads to the release of the autoinhibitory interface of SHP2, which in turn renders the SHP2 PTP active and available for substrate recognition and reaction catalysis. The catalytic activity of SHP2 was monitored using the surrogate substrate DiFMUP in a prompt fluorescence assay format. More specifically, the phosphatase reactions were performed at room temperature in 384-well black polystyrene plate, flat bottom, low flange, nonbinding surface (Corning, cat. no. 3575) using a final reaction volume of 25 μL and the following assay buffer conditions: 60 mM HEPES, pH 7.2, 75 mM NaCl, 75 mM KCl, 1 mM EDTA, 0.05% P-20, 5 mM DTT.

The inhibition of SHP2 from the tested compounds (concentrations varying from 0.003 to 100 μM) was monitored using an assay in which 0.5 nM of SHP2 was incubated with of 0.5 μM of peptide IRS1_pY1172(dPEG8)pY1222(sequence H2N-LN(pY)IDLDLV- (dPEG8)LST(pY)ASINFQK-amide). After 30−60 min incubation at 25 °C, the surrogate substrate DiFMUP (Invitrogen, cat. no. D6567, 200 μM) was added to the reaction and incubated at 25 °C for 30 min (200 μM for residue 2−593, 100 μM for residue 1−525 construct). The reaction was then quenched by the addition of 5 μL of a 160 μM solution of bpV(Phen) (Enzo Life Sciences cat. no. ALX-270−204).

The fluorescence signal was monitored using a microplate reader (Envision, Perki-Elmer) using excitation and emission wavelengths of 340 and 450 nm, respectively. The inhibitor dose−response curves were analyzed using normalized IC_{50} regression curve fitting with control based normalization.

Cellular Assay. *p-ERK* cellular assay using the AlphaScreen SureFire Phospho-ERK 1/2 Kit (PerkinElmer) was performed as follows: KYSE-520 cells (30,000 cells/well) were grown in 96-well plate culture overnight and treated with SHP2 inhibitors at concentrations of 20, 6.6, 2.2, 0.74, 0.24, 0.08, and 0.027 μM for 2 h at 37 °C. Incubations were terminated by addition of 30 μL of lysis buffer (PerkinElmer) supplied with the SureFire phospho-extracellular signal-regulated kinase (*p-ERK*) assay kit (PerkinElmer). Samples were processed according to the manufacturer's directions. The fluorescence signal from *p-ERK* was measured in duplicate using a 2101 multilabel reader (PerkinElmer Envision). The percentage of inhibition was normalized by the total ERK signal and compared with the DMSO vehicle control.

Cell Proliferation Assay. Cells (1500-cells/well) were plated onto 96-well plates in 100 μL medium (RPMI-1640 containing 10% FBS, Lonza). Compounds with various concentrations (1.25, 2.5, 5, 10, and 20 μM) were added 24 h after cell plating. At day 5, 50 μL of Celltiter-Glo reagent (Promega) was added, and the luminescent signal was determined according to the supplier's instruction (Promega).

Selectivity Assays. Activity of **1** vs a panel composed of select GPCR, ion channel, nuclear receptor, transporter, enzyme and kinase targets is provided in the Supporting Information.

Differential Scanning Fluorimetry. (DSF) was used as a method to identify compounds that stabilize SHP2 from thermal denaturation. The following assay conditions were used: 100 μg/mL

SHP2, 5× SYPRO Orange dye (5000× concentrate in DMSO; Life Technologies), 100 mM Bis-Tris (pH 6.5), 100 mM NaCl, 0.25 mM TCEP, and 5% DMSO. The final compound concentration evaluated was 100 μM. To carry out the experiment, 9.5 μL of DSF assay solution was dispensed into an assay plate (LightCycler; 480 multiwell plate 384 white) containing 500 nL of compound dissolved in DMSO then mixed. The final assay volume was 10 μL per well in a 384-well format. Plates were then sealed after reagent addition, centrifuged at 1000 rpm for 1 min, and read on a Bio-Rad C1000 thermal cycler with a CFX384 real time system using an excitation of 465 nm and an emission at 580 nm. The temperature was ramped from 25 to 75 °C, and measurements were taken at 0.5 °C increments. The melting temperature (T_m) of the raw fluorescence data was identified as the midpoint of the transitions via a semiparametric fit. The ΔT_m was determined by comparing the individual Tm values for each compound with the mean T_m of the apo SHP2 protein controls (32 per plate) containing DMSO only.

Crystallization and Structure Determination. Sitting drop vapor diffusion method was used for crystallization, with the crystallization well containing 17% PEG 3350 and 200 mM ammonium phosphate and a drop with a 1:1 volume of SHP2 protein and crystallization solution. Crystals were formed within 5 days and subsequently soaked in the crystallization solution with 2.5 mM of X. This was followed by cryoprotection using the crystallization solution with the addition of 20% glycerol and 1 mM of compounds **1**, **3**, **4**, **5**, or **24**, followed by flash freezing directly into liquid nitrogen.

Diffraction data for the SHP2/compound **2** complex is reported elswhere,[10] and those for SHP2/compound **1**, **3**, **4**, **5**, and **24** complexes were collected on a Dectris Pilatus 6M detector at beamline 17ID (IMCA-CAT) at the Advanced Photon Source at Argonne National Laboratories. The data were measured from a single crystal maintained at 100 K at a wavelength of 1 Å, and the

reflections were indexed, integrated, and scaled using XDS.24 The spacegroup of the complex was P21 with two molecules in the asymmetric unit. The structure was determined with Fourier methods, using the SHP2 apo structure1 (PDB accession 2SHP) with all waters removed. Structure determination was achieved through iterative rounds of positional and simulated annealing refinement using BUSTER,25 with model building using COOT.26 Individual B-factors were refined using an overall anisotropic B-factor refinement along with bulk solvent correction. The solvent, phosphate ions, and inhibitor were built into the density in later rounds of the refinement. Data collection and refinement statistics are shown in Tables 1, 2 of the Supporting Information.

Pharmacophore model. A consensus pharmacophore tool with ICM v.3.7-2d was used for visualization based on ligand structures from SHP2 crystal structures with **1**, **2**, and **3**.

Docking models. An initial structure of **15** was modeled from the crystal structure of **1** (PDB: *6MDC*), and R111 conformation was modeled based on a previous observation from SHP099 (PDB: *5EHR*) for a hydrogen bond. Protein force field parameters were assigned with the protein preparation tool with Maestro v.2014-2 (Schrodinger). Then, the structure was energy minimized with MacroModel BatchMin v.10.4. **18** was modeled from the **20** crystal structure, then minimized with MacroModel. A low energy conformation around the thioether group of **23** was obtained with B3LYP/6-31G(d,p) with IEF-PCM water model using Gaussian 03. An initial complex model of **23** was built based on rigid molecule overlay to the SHP2-**20** structure using the low energy conformation of **23**. Then, the complex was relaxed using MacroModel using 10kJ/mol/Å2 restraint energy on the low energy conformation of thioether derived from Gaussian 03.

Pharmacokinetics. All animal related procedures were conducted under a Novartis IACUC approved protocol in compliance with Animal Welfare Act regulations and the Guide for the Care

and Use of Laboratory Animals. Male C57BL/6 mice were obtained from Harlan Laboratories. Following iv administration (via tail vein) at 1 mg/kg, approximately 50 μL of whole blood was collected via tail transection, at 0.083, 0.5, 1, 2, 4, and 7 h postdose and transferred to an Eppendorf microcentrifuge tube containing EDTA. Oral administration (at 5 mg/kg) and collection procedures were similar to IV, except with wholeblood collection at 0.25, 0.5, 1, 2, 4, and 7 h. The blood was centrifuged at 5000 rpm, and plasma was transferred to a Matrix 96 well plate, capped, and stored frozen (−20 °C) for parent compound analysis. Samples were precipitated and diluted with acetonitrile containing internal standard and prepared for LC/MS/MS. An aliquot (20 μL) of each sample was injected into an API4000 LC/MS/MS system for analysis, and transitions of 352.05 amu (Q1) and 267.10 amu (Q3) were monitored. All pharmacokinetic (PK) parameters were derived from concentration−time data by noncompartmental analyses. All PK parameters were calculated with the computer program WinNonlin (Version 6.4) purchased from Certara Company (St. Louis, MO). For the intravenous dose, the concentration of unchanged compound at time 0 was calculated based on a log−linear regression of first two data points to back-extrapolate C(0). The area under the concentration−time curve (AUC_{last}) was calculated using the linear trapezoidal rule. The bioavailability was estimated as following equation:

$$\%F = \frac{AUC_{\inf,p.o.}}{AUC_{\inf,i.v.}} \cdot \frac{Dose_{i.v.}}{Dose_{p.o.}}$$

Results are expressed as mean. No further statistical analysis was performed.

Tumor Xenograft Experiments. All animal studies were carried out according to the Novartis Guide for the Care and Use of Laboratory Animals. Six-week old female athymic NU/NU mice (Charles River Labs, MA), were inoculated subcutaneously with KYSE520 esophageal carcinoma cells (ATCC) at a concentration of 2 x 10^6 in a suspension containing 50% phenol red-free

matrigel (BD Biosciences) in Hank's balanced salt solution. For PK/PD studies, mice were administered a single dose of vehicle control (0.5% Methylcellulose, 0.1% Tween 80) or **14** by oral gavage once tumors reached roughly 300 mm^3. Mice were subsequently euthanized at predetermined time points following a single dose of compound at which point plasma and xenograft fragments were harvested for determination of **14** concentrations and PD modulation. Phospho-ERK PD assessment was carried on lysed frozen tumor tissue fragments following the protocol provided by the Mesoscale Discovery assay whole cell lysis kits (Catalog#: Total ERK1/2: K151DXD, phospho-ERK1/2: K151DWD). Protein concentration was assessed by BCA (Pierce, Catalog # 23225) and 2.5mg, for total-ERK, or 20 mg for phospho-ERK, were loaded onto mesoscale plates. Samples were analyzed by a Mesoscale plate reader. Data was analyzed and fold change in phospho-ERK1/2 levels were calculated by normalizing to total ERK concentrations and the ratio of phospho-ERK/total-ERK in the vehicle treated group. DUSP6 PD assessment was carried out by quantitative real-time PCR. Frozen tumor fragments were processed to extract mRNA (Qiagen #74106). RNA quantification was performed using Nanodrop 8000. One-step qPCR (Qiagen, #204645) was performed on the 7900 HT Fast Real-Time PCR system (Themo Fisher Scientific) using a human DUSP6 primer set (Hs00737962, Life Technologies) multiplexed with a housekeeping gene control primer, HPO (#4326314E, Life Technologies). Data was analyzed and normalized to the expression of a housekeeping gene, human ribosomal protein lateral stalk subunit P0, HPO, in order to calculate the fold change in mRNA expression with and without **14**.

ASSOCIATED CONTENT

Supporting Information.

The Supporting Information is available free of charge on the ACS Publications website at DOI: (insert DOI here), containing X-ray data tables, selectivity panel data for **1;** PK profiles for **1**, **5**, **14**; synthetic procedures; Molecular Formula Strings, docking models (Figures 2-4).

Accession Codes

6MD9 for SHP2 in complex with compound **3**; *6MDA* for SHP2 in complex with compound **4**; *6MDB* for SHP2 in complex with compound **5**; *6MDD* for SHP2 in complex with compound **24**; *6MDC* for SHP2 in complex with compound **1**. Authors will release the atomic coordinates and experimental data upon article publication

AUTHOR INFORMATION

Corresponding Author. E-mail: matthew.lamarche@novartis.com. Telephone: 617-871-7729. 250 Massachusetts Avenue, Cambridge, Massachusetts, 02139, United States.

Author Contributions. The manuscript was written through contributions of all authors. All authors have given approval to the final version of the manuscript.

Notes. The authors declare no competing financial interest.

ACKNOWLEDGEMENTS. Use of the IMCA-CAT beamline 17-ID at the Advanced Photon Source was supported by the companies of the Industrial Macromolecular Crystallography Association through a contract with Hauptman-Woodward Medical Research Instituted. Use of the Advanced Photon Source was supported by the U.S. Department of Energy, Office of Science, Office of Basic Energy Sciences, under Contract No. DE-AC02-06CH11357. The authors thank Yue Pan, Dan Palacios, Joe Wzorek, Jonathan Hempel for editing suggestions, and the entire SHP2 team.

ABBREVIATIONS USED. PTP, protein tyrosine phosphatase; RAS, rat sarcoma protein; AKT, protein kinase B; JAK, Janus kinase; STAT, signal transducer and activator of transcription proteins; ERK, extracellular signal-regulated kinase; PI3K, phosphoinositide 3-kinase; MAPK, mitogen-activated protein kinase; TCEP, tris(2-carboxyethyl)phosphine; IPTG, isopropyl β-D-1-thiogalactopyranoside; EDTA, ethylenediaminetetraacetic acid; HEPES, 4-(2-hydroxyethyl)-1-piperazineethanesulfonic acid; DTT, dithiothreitol

REFERENCES

1. Tartaglia, M.; Niemeyer, C. M.; Fragale, A.; Song, X.; Buechner, J.; Jung, A.; Hählen, K.; Hasle, H.; Licht, J. D.; Gelb, B. D. Somatic Mutations in PTPN11 in Juvenile Myelomonocytic Leukemia, Myelodysplactic Syndromes and Acute Myeloid Leukemia. *Nat. Genet.* **2003**, *34*, 148-150.

2. a) Chan, G.; Kalaitzidis, D.; Neel, B. G. The Tyrosine Phosphoatase Shp2 (*PTPN11*) in Cancer. *Cancer Metastasis Rev.* **2008**, *27*, 179-192. b) Miyamoto, D.; Miyamoto, M.; Takahashi, A.; Yomogita, Y.; Hagashi, H.; Kondo, S.; Hatakeyama, M. Isolation of a Distinct Class of Gain-of-Function SHP-2 Mutants with Oncogenic RAS-like Transforming Activity From Solid Tumors. *Oncogene*, **2008**, *27*, 3508-3515.

3. Plusky, S.; Wandless, T. J.; Walsh, C. T.; Shoelson, S. E.; Potent Stimulation of SH-PTP2 Phosphatase Activity by Simultaneous Occupancy of Both SH2 Domains. *J. Biol. Chem.*, **1995,** *270*, 2897-2900.

4. a) Neel, B. G.; Gu, H.; Pao, L. The 'Shp'ing News: SH2 Domain-Containing Tyrosine Phosphatases in Cell Signaling. *Trends Biochem. Sci.*, **2003**, *28*, 284-293. b) Chan, R. J.; Feng, G. S. PTPN11 is the First Identified Proto-Oncogene That Encodes a Tyrosine

Phosphatase. *Blood* **2007**, *109*, 862-867. c) Tiganis, T.; Bennett, A. M. Protein Tyrosine Phosphatase Function: the Substrated Perspective. *Biochem. J.* **2007**, *402*, 1-15. d) Vazhappilly, C., G.; Saleh, E.; Ramadan, W.; Menon, V.; Al-Azawi, A. M.; Tarazi, H.; Abdu-Allah, H.; El-Shorbagi, A.-N.; El-Awady, R. Inhibition of SHP2 by New Compounds Induces Differential Effects on RAS/RAF/ERK and PI3K/AKT Pathways in Different Cancer Cell Types. *Invest. New Drugs* **2018**, ahead of print. doi: 10.1007/s10637-018-0626-5. e) Wong, S. G.; Zhou, J.; Liu, J. B.; Wu, Z.; Xu, X.; Li, T.; Xu, D.; Schumacher, S. E.; Puschhof, J.; McFarland, J.; Zou, C.; Dulak, A.; Henderson, L.; Xu, P.; O'Day, E.; Rendak, R.; Liao, W.-L.; Cecchi, F.; Hembrough, T.; Schwartz, S.; Szeto, C.; Rustgi, A. K.; Wong, K.-K.; Diehl, J. A.; Jensen, K.; Graziano, F.; Ruzzo, A.; Fereshetian, S.; Mertins, P.; Carr, S. A.; Beroukhim, R.; Nakamura, K.; Oki, E.; Watanabe, M.; Baba, H.; Imamura, Y.; Catenacci, D.; Bass, A. J. Targeting Wild-type KRAS-Amplified Gastroesophageal Cancer Through Combined MEK and SHP2 Inhibition. *Nat. Med.* **2018**, *24*, 968-977. f) Mainardi, S.; Mulero-Sánchez, A.; Prahallad, A.; Germano, G.; Bosma, A.; Krimpenfort, P.; Lieftink, C.; Steinberg, J. D.; de Wit, N.; Gonçalves-Ribeiro, S.; Nadal, E.; Bardelli, A.; Villanueva, A.; Bernards., R. SHP2 is Required for Growth of KRAS-Mutant Non-Small-Cell Lung Cancer In Vivo. Nat. Med. **2018**, *24*, 961–967.

5. Bunda, S.; Burrell, K.; Heir, P.; Zeng, L.; Alamsahebpour, A.; Kano, Y.; Raught, B.; Zhang, Z–Y.; Zadeh, G.; Ohh, M.; Inhibition of SHP2–Mediated Dephosphorylation of Ras Suppresses Oncogenesis. *Nat. Commun.*, **2015**, *6*, 8859, DOI: 10.1038/ncomms9859.

6. Li, J.; Jie, H.-B.; Lei, Y.; Gildener-Leapman, N.; Trivedi, S. PD-1/SHP-2 Inhibits Tc1/Th1 Phenotypic Responses and the Activation of T Cells in the Tumor Microenvironment. *Cancer Res.* **2015**, *75*, 508-518.

7. Hui, E.; Cheung, J.; Zhu, J.; Su, X. ; Taylor, M.J.; Wallweber, H.A.; Sasmal, D.K.; Huang, J.; Kim, J.M.; Mellman, I.; Vale, R.D. T Cell Costimulatory Receptor CD28 is a Primary Target for PD-1-Mediated Inhibition. *Science*, **2017**, 1428-1433, DOI: 10.1126/science.aafl292

8. (a) Topalian, S.L.; Hodi, F.S; Brahmer, J.R.; Gettinger, S.N.; Smith, D.C.; McDermott, D.F.; Powderly, J.D.; Carvajal, R.D.; Sosman, J.A.; Atkins, M.B.; Leming, P.D.; Spigel, D.R.; Antonia, S.J.; Horn, L.; Drake, C.G.; Pardoll, D.M.; Chen, L.; Sharfman, W.H.; Anders, R.A.; Taube, J.M.; McMiller, T.L.; Xu,H.; Korman, A.J.; Jure-Kunkel, M.; Agrawal, S.; McDonald, D.; Kollia, G.D.; Gupta, A.; Wigginton, J.M.; Sznol, M. Safety, Activity, and Immune Correlates of Anti-PD-1 Antibody in Cancer. *New Engl. J. Med.,* **2012**, *366*, 2443–2454. (b) Ohigashi, Y.; Sho, M.; Yamada, Y.; Tsurui, Y.; Hamada, K.; Ikeda, N.; Mizuno, T.; Yoriki, R.; Kashizuka, H.; Yane, K.; Tsushima, F.; Otsuki, N.; Yagita, H.; Azuma, M.; Nakajima, Y.; Clinical Significance of Programmed Death-1 Ligand-1 and

Programmed Death-1 Ligand-2 Expression in Human Esophageal Cancer. *Clin. Cancer Res.,* 2005, *11*, 2947–2953.

9. Butterworth, S.; Overduin, M.; Barr, A. J. Targeting Protein Tyrosine Phosphatase SHP2 for Therapeutic Intervention. *Future Med. Chem.* **2014**, *6*, 1423-1437.

10. Chen, Y.P.; LaMarche, M.J.; Fekkes, P.; Garcia–Fortanet, J.; Acker, M.; Chan, H.; Chen, Z.; Deng, Z.; Fei, F.; Firestone, B.; Fodor, M.; Gao, H.; Ho, S.; Hsiao, K.; Kang, Z.; Keen, .N; Labonte, L.; Liu, S.; Meyer, M.; Pu, M.; Price, E.; Ramsey, T.; Slisz, J.; Wang, P.; Yang, G.; Zhang, J.; Zhu, P.; Sellers, W.R.; Stams, T.; Fortin, P.D. Discovery of an Allosteric SHP2 Inhibitor for Cancer Therapy. *Nature*, **2016**, *535*, 148–152.

11. Fodor, M.; Price, E.; Wang P.; Lu H.; Argintaru A.; Chen Z.; Glick M.; Hao H.; Kato, M.; Koenig, R.; LaRochelle, J.R.; Liu, G.; McNeill, E,; Majumdar, D.; Nishiguchi, G.A.; Perez, L.B.; Paris, G.; Quinn, C.M.; Ramsey, T.; Sendzik, M.; Shultz, M.D.; Williams, S.L.; Stams, T.; Blacklow, S.C.; Acker, M.G.; LaMarche M.J.; Dual Allosteric Inhibition of SHP2 Phosphatase. *ACS Chem. Biol*. **2018**, 13, 647-656. doi: 10.1021/acschembio.7b00980

12. Fortanet, J. G.; Chen, C. H.-T.; Chen, Y.-N. P.; Chen, Z.; Deng, Z.; Firestone, B.; Fekkes, P.; Fodor, M.; Fortin, P. D.; Fridrich, C.; Grunenfelder, D.; Ho, S.; Kang, Z. B.; Karki, R.; Kato, M.; Keen, N.; LaBonte, L. R.; Larrow, J.; Lenoir, F.; Liu, G.; Liu, S.; Lombardo, F.; Majumdar, D.; Meyer, M. J.; Palermo, M.; Perez, L.; Pu, M.; Ramsey, T.; Sellers, W. R.; Shultz, M. D.; Stams, T.; Towler, C.; Wang, P.; Williams, S. L.; Zhang, J.-H.; LaMarche, M. J. Allosteric Inhibition of SHP2: Identification of a Potent, Selective, and Orally Efficacious Phosphatase Inhibitor. *J. Med. Chem.* **2016,** *59*, 7773-7782.

13. (a) Hof, P.; Pluskey, S.; Dhe-Paganon, S.; Eck, M. J.; Shoelson, S. E. Crystal Dtructure of the Tyrosine Phosphatase SHP-2. *Cell* **1998,** *92,* 441−450. (b) Barford, D.; Neel, B. G. Revealing Mechanisms for SH2 Domain Mediated Regulation of the Protein Tyrosine Phosphatase SHP-2. *Structure* **1998,** *6,* 249−254.

14. Novartis SHP2 patent applications: (a) Chen, Z.; Fortanet, J.G.; Grunenfelder, D.; Karki, R,; Kato, M,; LaMarche, M.J.; Perez, L. B.; Stams, T. M.; Williams, S.; 1 -Pyridazin-/triazin-3-yl-piper(-azine)/idine/pyrolidine Derivatives and Compositions Thereof for Inhibiting the Activity of SHP2. WO15107493, January 16, 2015. (b) Chen, Z.; Dore, M,; Fortanet, J.G.; Karki, R.; Kato, M.; LaMarche, M.J.; Perez, L.B.; Williams, S.; Sendzik, M. 1 -(Triazin-3-yl/pyridazin-3-yl)-piper(-azine)idine Derivatives and Compositions for Inhibiting the Activity of SHP2. WO15107494, January 16, 2015. (c) Chen, C.H.; Chen, Z.; Dore, M.; Fortanet, J.G.; Karki, R.; Kato, M.; LaMarche, M.J.; Perez, L.B.; Smith, T.; Williams, S.; Toure, B.B.; Sendzik, M.; N-azaspirocycloalkane Substituted N-Heteroaryl Compounds and Compositions for Inhibiting the Activity of SHP2. WO15107495, January 16, 2015. (d) Bagdanoff, J.T.; Chen, Z.; Dore, M.; Fortanet, J.G.; Kato, M.; LaMarche, M.J.; Sarver, P.J.; Shultz, M.; Smith, T.D.; Williams, S.; Ccompounds and Compositions for Inhibiting the Activity of SHP2. WO16203404, June 15, 2016. (e) Chen, Z.; Fortanet, J.G.; LaMarche, M.J.; Sendzik, M.; Tamez, V.; Yu, B.; Compounds and Compositions for Inhibiting the Activity of SHP2. WO16203405, June 15, 2016. (f) Chen, Z.; Fortanet, J.G.; Jouk, A.; Karki, R.; LaMarche, M.J.; Liu, G.; Palermo, M.; Perez, L.B.; Sarver, P.J.; Shultz, M.D.; Sendzik, M.; Toure, B.B.; Yu, B.; Compounds and Compositions for Inhibiting the Activity of SHP2. WO16203406, June 15, 2016. (g) Chen, Z.; Fortanet, J.G.; Karki, R.; LaMarche, M.J.; Majumdar, D.; Perez, L.B.; Sendzik, M.; Smith, T.D.;

Yang, F.; Yu, B. Compounds and Compositions for Inhibiting the Activity of SHP2. WO17216706, June 12, 2017.

15 (a) Flemming, Alexandra. Allosteric Phosphatase Inhibitor Puts Brake on Cancer Cells. Nature Reviews Drug discovery, 2016, 15, 530-531. (b) Batth, T.S.; Papetti, M.; Pfeiffer, A.; Tollenaere, M.A.X.; Francavilla, C.; Olsen, J.V.; Large-Scale Phosphoproteomics Reveals Shp-2 Phosphatase-Dependent Regulators of Pdgf Receptor Signaling. *Cell reports*, 22, 2784-2796. (c) Jin, W.Y.; Ma, Y.; Li, W.; Li, H.L.; Wang, R.L. Scaffold-Based Novel SHP2 Allosteric Inhibitors Design Using Receptor-Ligand Pharmacophore Model, Virtual Screening and Molecular Dynamics. Computational Biology and Chemistry. **2018**, 73, 179-188. (d) Dardaei, L.; Wang, H.Q.; Singh, M.; Fordjour, P.; Shaw, K.X.; Yoda, S.; Kerr, G.; Yu, K.; Liang, J.; Cao, Y.; Yichen; Chen, Y.; Lawrence, M.S.; Langenbucher, A.; Gainor, J.F.; Friboulet, L.; Dagogo-J.I.; Myers, D.T.; Labrot, E.; Ruddy, D.; Parks, M.; Lee, D.; Di Cecca, R.H.; Moody, S.; Hao, H.; Mohseni, M.; LaMarche, M.; Williams, J.; Hoffmaster, K.; Caponigro, G.; Shaw, A.T.; Hata, A.N.; Benes, C. H.; Li, F.; Engelman, J.A. SHP2 Inhibition Restores Sensitivity in ALK-Rearranged Non-Small-Cell Lung Cancer Resistant to ALK Inhibitors. *Nature Medicine,* **2018**, 24, 512-517. (e) Sun, X.; Ren, Y.; Gunawan, S.; Teng, P.; Chen, Z.; Lawrence, H. R.; Cai, J.; Lawrence, N. J.; Wu, J. Selective Inhibition of Leukemia-Associated SHP2E69K Mutant by the Allosteric SHP2 Inhibitor SHP099 *Leukemia,* 2018, 32, 1246-1249. (f) Kostallari, E.; Hirsova, P.; Prasnicka, A.; Verma, V.K.; Yaqoob, U.; Wongjarupong, N.; Roberts, L.R.; Shah, V.H. Hepatic Stellate Cell-Derived Platelet-Derived Growth Factor Receptor-Alpha-Enriched Extracellular Vesicles Promote Liver Fibrosis in Mice Through SHP2. *Hepatology,* **2018**, 68, 333-348. (g) LaRochelle, J.R.; Fodor, M.; Vemulapalli, V.; Mohseni, M.; Wang, P.; Stams, T.;

LaMarche, M.J.; Chopra, R.; Acker, M.G.; Blacklow, S.C; Structural Reorganization of SHP2 by Oncogenic Mutations and Implications for Oncoprotein Resistance to Allosteric Inhibition. *Nat. Commun*. **2018**, 4508. doi: 10.1038/s41467-018-06823-9.

(h) Pádua, R.A.P.; Sun, Y.; Marko, I.; Pitsawong, W.; Stiller, J.B.; Otten, R.; Kern, D.; Mechanism of Activating Mutations and Allosteric Drug Inhibition of the Phosphatase SHP2. *Nat. Commun.* **2018**, 4507. DOI: 10.1038/s41467-018-06814-w.

16. (a) Czako, B.; Jones, P.; Cross, P.; Leonard, P.; Heterocyclic Inhibitors of PTPN11. University of Texas, WO2017156397, March 10, 2017. (b) Zhu, J.; Gu, S.; Si, X.; Xie, J.; Shen, J.; N-Heterocyclic Ring Compound, and Intermediate, Preparation Method, Medicine Composition and Application Thereof. Shanghai Organic Institute CN107286150, October 24, 2017.

17. (a) Ma, C.; Gao, P.; Chu, J.; Wu, X.; Wen, C.; Kang, D.; Bai, J.; Pei, X.; Novel Heterocyclic Derivatives Useful as SHP2 Inhibitors. Jacobio, WO2017211303, June 7, 2017. (b) Jogalekar, A.; Won, W.; Koltun, E.S.; Gill, A.; Mellem, K.; Aay, N.; Buckl, A.; Semko, C.; Kiss, G.; 2,5-Disubstituted 3-Methyl Pyrazines and 2,5,6-Trisubstituted 3-Methyl Pyrazines As Allosteric SHP2 Inhibitors. Revolution Medicines, WO2018013597, July 11, 2017. (c) Gill, A.; Aay, N.; Mellem, K.; Buckyl, A.; Koltun, E.S.; Semko, C.; Kiss, G.; Pyridine Compounds as Allosteric SHP2 Inhibitors. Revolution Medicines, WO2018136264, January 9, 2018. (d) Blank, B.R.; Pitzen, J.; Wang, G.; Won, W.S.; Tzitzilonis, C.; Li, J.J.; Koltun, E.S.; Aay, N.; Buckyl, A.; Mellem, K.; Semko, C.; Jogalekar, A.; Kiss, G.; Gill, A.; Bicyclic Compounds as Allosteric SHP2 Inhibitors. Revolution Medicines, WO2018136265, January 9, 2018. (e) Albrecht, B.K.; Giordanetto, F.; Greisman, J.B.; Maragakis, P.; Taylor, A.M.; Walters, W.P.; SHP2 Phosphatase

Inhibitors and Methods of Use Thereof. Relay Therapeutics, WO2018057884, September 22, 2017. (f) Giordanetto, F.; Greisman, J.B.; Maragakis, P.; Taylor, A.M.; Dipietro, L.V.; Kelley, E.H.; Lescarbeau, A.; Murcko, M.A.; Pierce, L.C.T.; Shortsleeves, K.C.; Walters, W.P.; Bhat, S.; Therrien, E.; Dahlgren, M.K.; Pyrazolo[3,4-B]Pyrazine Derivatives as SHP2 Phosphatase Inhibitors. Relay Therapeutics, WO2018081091, October 24, 2017. (g) Taylor, A.M.; Lescarbeau, A.; Kelley, E.H.; Shortsleeves, K.C.; Dipietro, L.V.; Walters, W.P.; Murcko, M.A.; Pierce, L.C.; Tang, Y.; Giordanetto, F.; Greisman, J.B.; Maragakis, P.; Bhat, S.; Dahlgeren, M.K.; Therrien, E.; Pyrazolo[3,4-B]Pyrazine Derivatives as SHP2 Phosphatase Inhibitors. Relay Therapeutics, WO2018218133, May 25, 2018. (h) Nichols, R.J.; Haderk, F.; Stahlhut, C.; Schulze, C.J.; Hemmati, G.; Wildes, D.; Tzitzilonis, C.; Mordec, K.; Marquez, A.; Romero, J.; Hsieh, T.; Zaman, A.; Olivas, V.; McCoach, C.; Blakely, C.M.; Wang, Z.; Kiss, G.; Koltun, E.S.; Gill, A.L.; Singh, M.; Goldsmith, M.A.; Smith, J.A.M.; Bivona, T.G.; RAS Nucleotide Cycling Underlies the SHP2 Phosphatase Dependence of Mutant BRAF-, NF1- and RAS-Driven Cancers. *Nat Cell Biol.* **2018**, 1064-1073. doi: 10.1038/s41556-018-0169-1.

18. Sarver, P.; Acker, M.; Bagdanoff, J.T.; Chen, Z.; Chen, Y.N.; Chan, H.; Firestone, B.; Fodor, M.; Garcia-Fortanet, J.; Hao, H.; Hentemann, M.; Kato, M.; Koenig, R.; LaBonte, L.R.; Liu, G.; Liu, S.; C. Liu; McNeil, E.; Mohseni, M.; Sendzik, M.; Stams, T.; Spence, S.; Tamez, V.; Tichkule, R.; Towler, C.; Wang, H.; Wang, P.; Williams, S.L.; Yu, B.; LaMarche, M.J. 6-Amino-3-Methylpyrimidinones as Potent, Selective, and Orally Efficacious SHP2 Inhibitors. *J. Med. Chem*., **2018**, companion manuscript jm-2018-017268 to be published in same issue.

19. Fitch, C. A.; Platzer, G.; Okon, M.; Garcia-Moreno E. B.; McIntosh, L. P. Arginine: Its pKa Value Revisited. Protein Sci. **2015**, *24*, 752-761.

20. The synthesis of spirocyclic amines is included in the SI for this manuscript. They may also be found at: (a) Zhuoliang; C.; Fortanet, J. G.; LaMarche, M. J.; Sendzik, M.; Tamez, V.; Bing, Y. Preparation of Substituted Pyrimidinones for Inhibiting the Activity of SHP2. WO2016203405, December 22, 2016. (b) Bagdanoff, J. T.; Chen, Z.; Dore, M.; Fortanet, J. G.; Kato, M.; LaMarche, M. J.; Sarver, P. J.; Shultz, M.; Smith, T. D.s; Williams, S. Preparation of Substituted Pyrazolopyrimidinones and Pyrrolopyrimidinones for Inhibiting the Activity of SHP2. WO2016203404, December 22, 2016.